

The 19 June 2002 “Mantle Echo” Case: Sensitivity to Microphysics and Convection Initiation

Robert G. Fovell^{1*} and Axel Seifert²

¹UCLA Atmospheric and Oceanic Sciences, Los Angeles, California, USA

²Deutscher Wetterdienst, Offenbach, Germany

1. Introduction

Recently, Wakimoto et al. (2004; “WMFL”) presented finescale radar observations of the very early stages of precipitation formation in developing deep convection. The echoes in two cases first appeared well above the ground, and took on an inverted “U” shape (hence, “mantle echo”). The study’s simulations used ARPS with the very common used, albeit simple, Lin et al. (1983; “LFO”) microphysical parameterization. The LFO scheme presumes exponential size distributions for precipitating particles having specified intercepts and densities. The default setup resulted in the early appearance of very bright echoes, located in the middle instead of upper troposphere. Considerable tweaking was needed to get results comparable to the observations with respect to echo brightness and first echo location.

We have revisited the 19 June 2002 mantle echo case using WRF and Seifert and Beheng’s (2005; “SB”) two-moment microphysics. The SB approach predicts the mass content L and number density N of hydrometeors (cloud droplets, cloud ice, rain, snow and graupel) separately. The convection’s early development is relatively insensitive to microphysics. Since that is not true of the storm’s subsequent evolution, these cases provide a very attractive platform for testing microphysical schemes and assumptions. We have also begun reconsidering the ubiquitous method for initiating convection in idealized simulations, the isolated buoyant thermal.

2. Initialization

On 19 June, a dryline extended through northwest Kansas, parallel to a cold front located just to the west. The sounding used for the WRF simulations (Fig. 1) was launched at 2003 UTC from a mobile platform situated just east of the dryline. Convec-

*Corresponding author address: Prof. Robert Fovell, UCLA Atmospheric and Oceanic Sciences, Los Angeles, CA 90095-1565. E-mail: rfovell@ucla.edu.

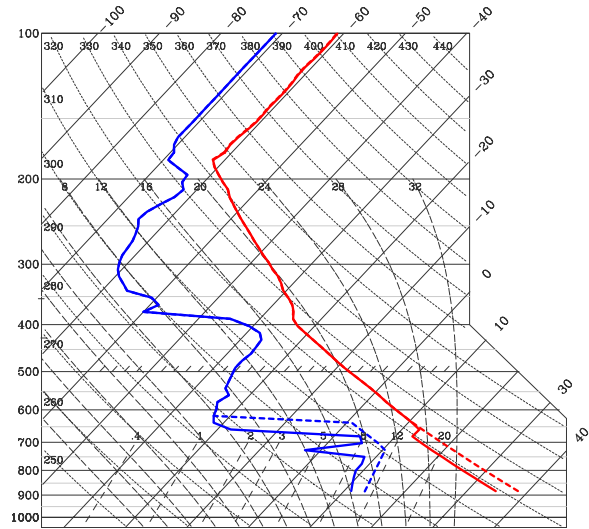


Fig. 1: Mobile sounding from 2003 UTC used in the 19 June 2002 WRF simulations. Superadiabatic layers were removed and a stratosphere was added.

tion fired up along this section of the dryline more than an hour later (WMFL Fig. 1). Note the inversion at 650 hPa. Figure 2, taken from WMFL, shows a vertical cross-section intersecting the two boundaries, made using dropsondes deployed just before convection started. Close to the dryline, the inversion was absent, and the moist layer was considerably deeper, both consequences of sustained lifting along the boundary. While convection was initiated above the dryline, the air involved was probably drawn from the lower troposphere east of the boundary (Murphey et al. 2005), where absolute humidities were higher (dashed arrow on Fig. 2).

These facts guided the construction of the initial perturbation used to excite convection. A 16 km wide “augmented environment” was inserted in the domain, characterized by the dashed curves on Fig. 1, to reflect the consequences of dryline-associated modification. The moisture increase there was considerably smaller than that contained in WMFL’s compact, moistened thermal so initiation was much

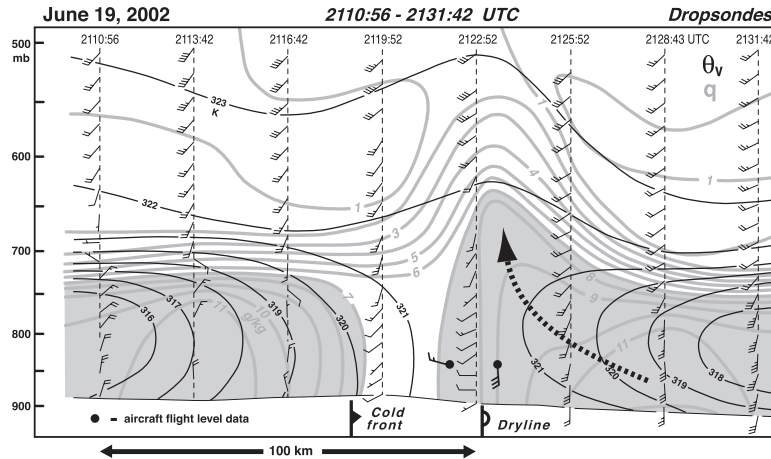


Fig. 2: Vertical cross-section of winds, virtual potential temperature (black 1 K contours) and mixing ratio (grey 1 g kg^{-1} contours) spanning the dryline, constructed from dropsondes. From Wakimoto et al. (2004).

slower and less impulsive. Results using a standard isolated thermal were also evaluated.

Simulations using the SB and the LFO schemes were made, the latter retaining default (untweaked) parameter values. Both runs were two-dimensional and employed version 2.0.3 of the WRF ARW core in a 302 x 81 domain with uniform 250 m resolution. Open lateral boundaries and the 1.5 order TKE sub-grid mixing parameterization were adopted. Unlike WMFL, the cloud to rain autoconversion process has been retained in these simulations. This process had very little impact on the results shown herein owing to the relatively minor moisture augmentation associated with the initial perturbation.

3. Results with the SB scheme

Figure 3 presents the SB run's simulated reflectivity field at 28 min, along with the observed field taken from WMFL. The plots share a common scale, aspect ratio and color table for positive reflectivity; the vertical velocity field for the simulation is also shown. Similarities include the presence of pronounced weak echo vault with strong ascent flanked by regions of higher echo brightness not exceeding 20 dBZ. As in the observation, reflectivity was largely confined above 7 km, with larger values in those portions of the echo at lower elevation and/or farther from the vault. Embedded vortical motions, qualitatively similar to those detected by radar (WMFL Fig. 6b), are seen.

As was the case in WMFL's simulation, the updraft resident in the echo vault represented a *secondary* development, with the flanking echo lobes being the consequences of the earliest convective thermal ca-

pable of reaching the upper troposphere. That impulse excited gravity waves which propagated away in both directions, with condensate particles growing to radar-detectable size along the way. Thus, this result is dynamically quite similar to WMFL's despite somewhat different initial perturbations. Figure 4 shows relative humidity fields at 11 min for these two approaches to initiation. WMFL's standard elliptical thermal essentially imposed a length scale onto the initial convection while the present initial condition spawned a series of small "bubbles" of various sizes. However, those bubbles subsequently competed and coalesced, and finally yielded a thermal that ascended vigorously through the troposphere, aided by the sounding's relatively low stability.

4. Comparison to the unadjusted LFO scheme and remaining issues

Figure 5a shows reflectivity and vertical velocity for a simulation comparable to Fig. 3b, but using the default setup of the LFO scheme. Note the color table has changed; Fig. 5b presents Fig. 3b's SB result with this new table. Dynamically, the two simulations are very similar; microphysics had not made much of a difference yet. In pointed contrast from the SB results, reflectivities in the LFO case are far larger. First echo was much earlier, and located much closer to the ground (not shown). Note also the weak echo vault is completely absent.

In WMFL's study, it wasn't clear if the rapid development of very bright echoes in the standard LFO setup was a consequence primarily of excessive precipitation mass accumulations or overly large predicted particle sizes, as those are convolved in the single-moment scheme. Figure 5c demonstrates that

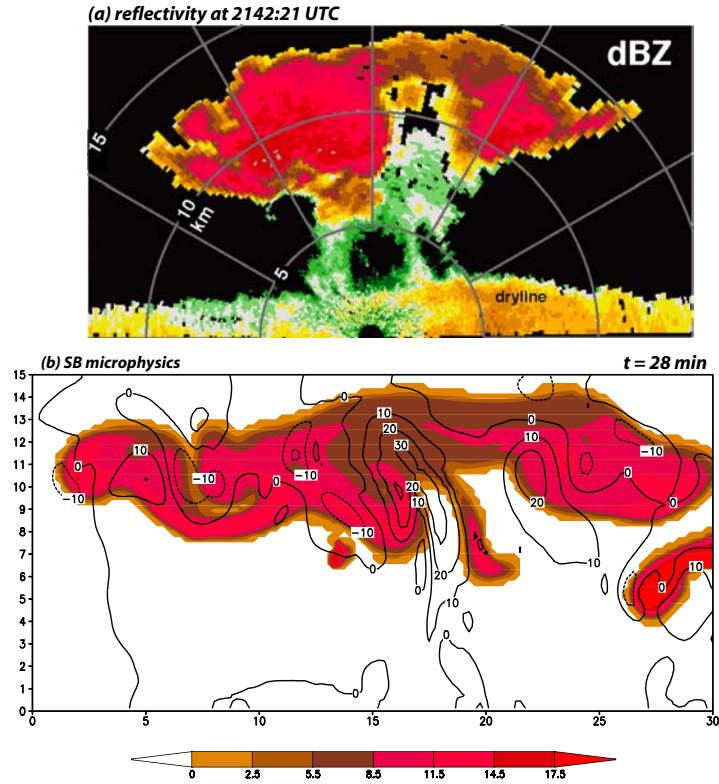


Fig. 3: Reflectivity fields observed (top) and simulated with SB microphysics. Plots share a common scale, aspect ratio and color table for positive reflectivities. Vertical velocity (10 m s^{-1} contours) shown on (b). Abscissa labels relative to plot left edge.

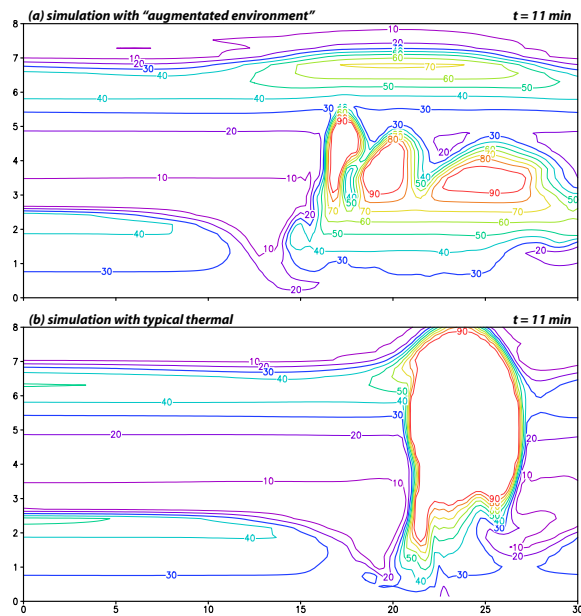


Fig. 4: Relative humidity contours (interval 10%) for "augmented environment" and standard thermal runs, after 11 min.

it was the latter by displaying a reflectivity field for the SB run but calculated using the *LFO scheme assumptions* regarding particle distribution parameters. By predicting both L and N , the SB approach can differentiate between grid volumes having a few large particles or many small ones for a given mass content, something the LFO scheme cannot do owing to its fixed intercept assumption. The combined mass contents of reflecting particles were roughly comparable in the two runs, but the fixed intercept assumption in LFO necessarily led to an overspecification of mean particle diameter, and thus echo brightness. Mean graupel particle diameters (not shown) were roughly a sixth as large with SB microphysics relative to default LFO, and that is what brought about the more realistic echo brightness.

WMFL's modifications to the LFO scheme were essentially designed to slow down accretion rates, delaying the conversion from non-reflecting particles (cloud water and ice) to visible radar targets such as snow and, ultimately, graupel. The present results show that slowing down accretion rates addressed the issue only indirectly. Still, there is a strong qualitative similarity between the SB approach and

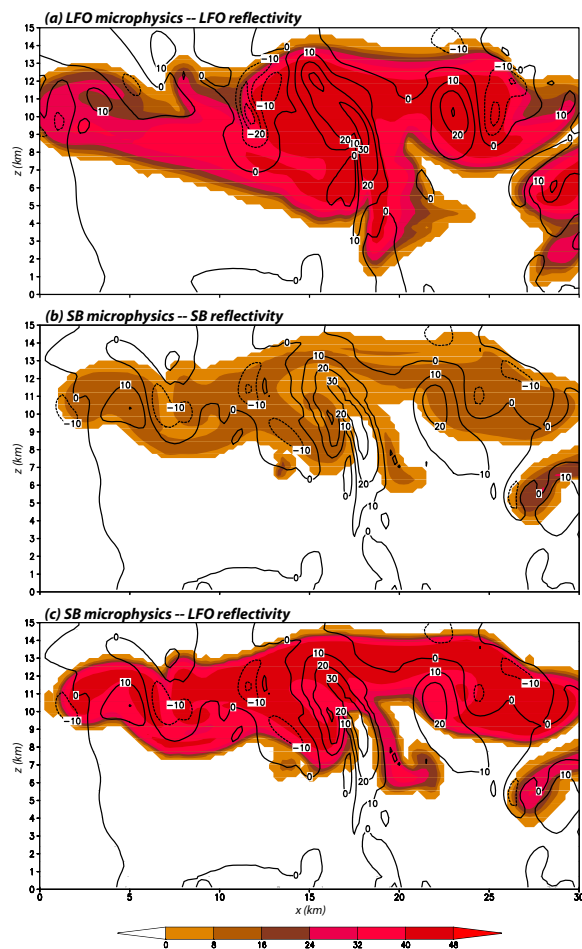


Fig. 5: Reflectivity fields for (a) default LFO, and (b) SB microphysics runs. For (c), SB run reflectivity was recomputed using LFO size distribution assumptions. Vertical velocity as in Fig. 3b.

WMFL's tweaked LFO results (not shown). Figure 6 presents snow and graupel fields at 28 min produced by the SB and default LFO schemes. In the former, graupel particles were generally found to reside in the lower portion of the echo, where indeed echo brightness was larger in both observations and the SB simulation (Fig. 3). The tweaked LFO scheme yielded qualitatively similar results. The default LFO scheme (Fig. 6b) produced much more graupel, spread throughout the cloud, including the main updraft.

5. Remaining issues and future work

With the present configuration and initialization, the SB run does not deliver precipitation to the ground. Even the default LFO run yielded little very rainfall. It is likely relevant that the portion of the dryline sampled by the mobile sounding and dropsondes proved to be a dramatic gap in the otherwise

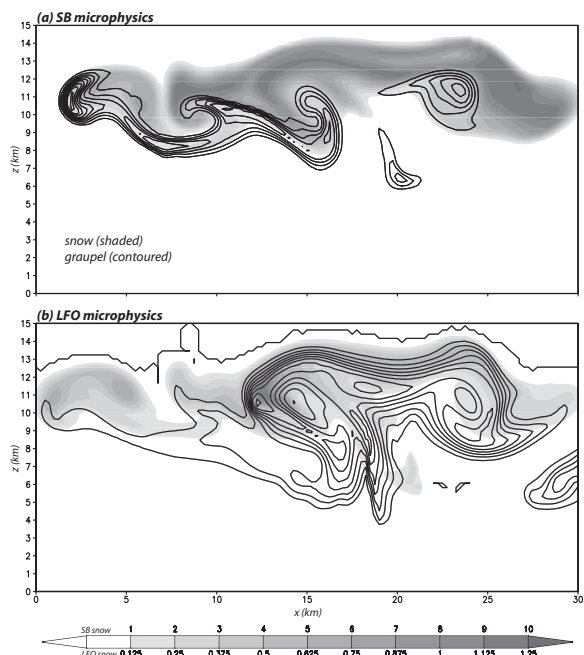


Fig. 6: Snow (shaded) and graupel (contoured) mass contents for the SB and default LFO runs. Graupel contour intervals 0.5 and 1 g kg^{-1} , respectively. Note color table shift.

extensive linear convection that developed. There is evidence of more substantial moisture elsewhere. More importantly, the cell in question traveled a substantial distance parallel the dryline during development, likely benefiting from sustained low-level forcing. We plan to incorporate similar forcing, probably using a momentum source as in Fovell (2005). We are also revisiting the other mantle echo case.

6. References

Fovell, R. G., 2005: Convective initiation ahead of the sea-breeze front *Mon. Wea. Rev.*, **133**, 264-278.

Lin, Y.-L., R. D. Farley, and H. D. Orville, 1983: Bulk parameterization of the snow field in a cloud model. *J. Climate Appl. Meteor.*, **22**, 1065-1092.

Murphey, H. V., R. M. Wakimoto, C. Flamant, and D. E. Kingsmill, 2005: Dryline on 19 June 2002 during IHOP. Part I: Airborne Doppler and LEANDRE II analyses of the thin line structure and convective initiation. *Mon. Wea. Rev.*, in press.

Seifert, A., and K. D. Beheng, 2005: A two moment cloud microphysics parameterization for mixed-phase clouds. Part I: Model description. *Meteor. Atmos. Phys.*, in press.

Wakimoto, R. M., H. V. Murphey, R. G. Fovell and W.-C. Lee, 2004 Mantle echoes associated with deep convection: Observations and numerical simulations. *Mon. Wea. Rev.*, **132**, 1701-1720.

Acknowledgments. This work was supported by NSF grant ATM-0139284.